



Since January 2020 Elsevier has created a COVID-19 resource centre with free information in English and Mandarin on the novel coronavirus COVID-19. The COVID-19 resource centre is hosted on Elsevier Connect, the company's public news and information website.

Elsevier hereby grants permission to make all its COVID-19-related research that is available on the COVID-19 resource centre - including this research content - immediately available in PubMed Central and other publicly funded repositories, such as the WHO COVID database with rights for unrestricted research re-use and analyses in any form or by any means with acknowledgement of the original source. These permissions are granted for free by Elsevier for as long as the COVID-19 resource centre remains active.



Solid-state ion-selective electrodes for the first potentiometric determination of the anti-COVID 19 drug Remdesivir in human plasma; A comparative study

Noha F. El Azab^{a,*}, Neven Ahmed^b

^a Pharmaceutical Analytical Chemistry Department, Faculty of Pharmacy, Ain Shams University, Organization of African Unity Street, Abbassia 11566, Cairo, Egypt

^b Egyptian Drug Authority, Giza, Egypt

ARTICLE INFO

Keywords:

Remdesivir
Graphene
Polyaniline nanoparticles
Ion selective electrode
Plasma
G/PANI nanocomposite

ABSTRACT

Establishing sensitive and targeted analytical methodologies for drug identification in biological fluids as well as screening of treatments that can counteract the most severe COVID-19 infection-related side effects are of utmost importance. Here, first attempts have been made for determination of the anti-COVID drug Remdesivir (RDS) in human plasma using four potentiometric sensors. Calixarene-8 (CX8) was used as an ionophore applied to the first electrode (Sensor I). The second had a layer of dispersed graphene nanocomposite coating (Sensor II). (Sensor III) was fabricated using nanoparticles of polyaniline (PANI) as ion-to-electron transducer. A reverse-phase polymerization using polyvinylpyrrolidone (PVP) was employed to create a graphene-polyaniline (G/PANI) nanocomposite electrode (Sensor IV). Surface morphology was confirmed by Scanning Electron Microscope (SEM). UV absorption spectra and Fourier Transform Ion Spectrophotometry (FTIR) also supported their structural characterization. The impact of graphene and polyaniline integration on the functionality and durability of the manufactured sensors was examined using the water layer test and signal drift. In the ranges of concentration of 10^{-7} to 10^{-2} mol/L and 10^{-7} to 10^{-3} , sensors II & IV exhibited linear responses; respectively while sensors I & III displayed linearity within 10^{-6} to 10^{-2} mol/L. The target drug was easily detectable using LOD down to 100 nmol/L. The developed sensors satisfactorily offered sensitive, stable, selective and accurate estimate of Remdesivir (RDS) in its pharmaceutical formulation as well as spiked human plasma with recoveries ranging from 91.02 to 95.76 % with average standard deviations less than 1.85. The suggested procedure was approved in accordance with ICH recommendations.

1. Introduction

As reported to the World Health Organization (WHO) in December 2019, COVID-19 arose in Wuhan, China, and subsequently spreaded throughout the world until being formally confirmed as a global epidemic on the 11th of March 2020. Many lives were lost, resulting in a negative effect on the world economy. Since then, there was a great desire for candidate therapeutics that target SARS-CoV-2 and associated symptoms in order to curb this pandemic [1]. Several drugs have been identified including Molnupiravir, Favipiravir, Ritonavir and Remdesivir (RDS).

(RDS) is a pro-drug nucleotide analogue that disrupts viral replication. It was tested in clinical studies to combat the 2014 Ebola outbreak. Fortunately, many virology laboratories examined (RDS) and

demonstrated that it could prevent coronavirus replication, including that of COVID-19. On October 22, 2020, the FDA approved the use of (RDS) for treating COVID-19, a hospital-required condition, in individuals over the age of 12 and in adults and children weighing at least 40 kg. On April 25, 2022, the FDA approved (RDS) as the first COVID-19 treatment for children under the age of 12 [2].

Several chromatographic [3–6], spectrophotometric [4,7] and voltammetric methods [8] have been reported for (RDS) analysis. However, to the best of our knowledge, no potentiometric methods have been developed yet for (RDS).

Potentiometric ion selective electrodes (ISE) are simple, low-cost sensors that can conduct measurements in turbid samples without the need for pre-treatment [9]. Solid contact (SC) electrodes are now widely employed and more preferable than the traditional liquid-contact

* Corresponding author.

E-mail address: noha.azab@pharma.asu.edu.eg (N.F. El Azab).

<https://doi.org/10.1016/j.microc.2023.108658>

Received 17 December 2022; Received in revised form 7 March 2023; Accepted 14 March 2023

Available online 21 March 2023

0026-265X/© 2023 Elsevier B.V. All rights reserved.

electrodes because they are simpler to construct and miniaturize [10]. However, SC sensors' main disadvantage is the electrode potential's tendency to fluctuate over time, necessitating the calibration of such sensors before each use. Their main benefit is the simplicity of use, transportation and storage [11].

Conducting polymers, carbon and other nanomaterials have enhanced SC electrodes' potential characteristics to attain stability and reproducibility, without the need for calibration and maintenance. These polymers are incorporated in between the solid contact and the ion selective membrane. The mobility of delocalized electrons in the polymer's conjugated structure, which transforms them into ion to electron transducers by doping, is what gives conducting polymers their electronic conductivity. Poly(o-aminophenol), polyaniline, poly(o-phenylenediamine), poly(N-phenylglycine), and other electrically conductive polymers have been used to stabilize the potential of solid-contact electrodes that are sensitive to specific drugs [12].

Among the most fundamental conducting polymers is polyaniline (PANI). This is due to simplicity in its synthesis, low cost, tunable conductivity, and excellent environmental stability. It benefits from metals' electrical conductivity and plastics' interesting characteristics, such as easy manufacturing and adjustable chemical and physical properties [13]. PANI has been utilized in a variety of applications where electrodes were electrochemically modified with PANI as an ion-to-electron transducer interlayer to improve the potential signal stability as in beverages and alcoholic drinks analysis [14], tramadol determination [15] where PANI had good pH stability and did not show any degradation of electrical response for 1 month. PANI was also used in determination of ascorbic acid [16] leading to improvement of the sensor performance and low detection limit and. PANI produced shorter response time for analysis of cephalosporin antibiotics [17] and provided high selectivity and sensitivity results for salicylates [18]. In glycopyrronium bromide analysis, PANI showed better results in terms of response time, potential drift and lifetime [19]. Also PANI maintained reproducible potentiometric signals over time in analysis of sulfacetamide and risedronate [20,21].

As ion to electron transducers in solid contact sensors, carbon-based nanomaterials such as single and multi-walled CNTs (MWCNTs), graphene, carbon black and fullerenes were also used. MWCNTs were employed as inner ion to electron transducing layer for anion detection in environmental samples [22] where MWCNTs generated more stable response. MWCNTs were also utilized in antipsychotic sulphiride sensor and succeeded in detecting low concentrations for long lifetime up to 22 weeks [23]. Graphene nanocomposite layer added more stability to electrode potential drift and short response times for metoclopramide analysis [24]. Graphene also provided longer lifetime of the sensor for monitoring mercury ions in waste water samples [25]. Graphene also generated the lowest detection limit and the longest lifetime when compared with other sensors for copper determination in real water samples and biological fluids [26].

Combining graphene with conducting polymers might result in a composite material with improved electrical conductivity and mechanical robustness owing to the synergistic findings of graphene and polyaniline as the graphene's incorporation in the solid-contact prevents water layer formation and enhances hydrophobicity [27]. However, it is essential to increase the PANI-graphene composites' processability and solvent dispersibility if they are to be used in more applications. So it is advisable that the dispersible PANI-graphene composites be made by first coating the aniline with graphene platelets, then aniline polymerization [28]. If the composite material is prepared in this fashion, it can be dissolved or dispersed in N-methylpyrrolidone (NMP) but not in water, which is better for applications where the aqueous liquids come into touch with composite material [29]. Graphene/PANI nanocomposite was only used once for potentiometric calcium determination where graphene's introduction into the transducer layer improved the initial potential stability and the response characteristics of the calcium solid contact ion selective electrode [27].

In this work we succeeded to prepare, for the first time, ISEs using graphene, PANI nanoparticles and Graphene-PANI nanocomposite as ion-to-electron transducers in SC sensors to selectively determine (RDS) in the presence of other anti-COVID drugs Favipiravir (FAV), Molnupiravir (MOL) and other interferants in pharmaceutical dosage forms and in human plasma. By contrasting them to a bare sensor devoid of an ion to electron transducer, the impact of their introduction on the potential stability taking into account shelf life and response time of the manufactured SC sensors was examined.

2. Experimental

2.1. Apparatus

For potential measurements, a digital ion analyzer (Jenway model 3330) obtained from (Essex, UK) and a Thermo Scientific Orion Ag/AgCl double junction reference electrode were both employed. A pH glass electrode (Jenway model number 924005-BO3-Q11C) from (Essex, UK) was utilized for pH adjustments.

A dual-beam UV-VIS spectrophotometer (Shimadzu model UV-1601 PC) from (Kyoto, Japan), was used to create UV-VIS spectra using 1-cm quartz cuvettes linked to a compatible computer (IBM) running UV-PC spectroscopy Shimadzu software version (3.7). Using a Centurion Centrifuge model K240R, PANI dispersion centrifugation was carried out (West Sussex, UK). Using a Malvern Zetasizer Nano-ZS, the Zeta potential of PANI particles was measured (Malvern Instruments Limited, Malvern, UK). Crest powerasonic CP500D ultrasonic cleaner (Malaysia) was used to homogenize the dispersion of graphene nanoplatelets.

A vortex mixer (model F20230176 ZX3) from Alfa medical Westbury (China), as well as a Bandelin Sonorex magnetic stirrer (model Rx 510 S) from (Budapest, Hungary) were additional equipments for solution stirring.

2.2. Materials

2.2.1. Reference samples

Remdesivir (RDS), Oseltamivir phosphate, Favipiravir and Molnupiravir were kindly donated by Apex pharma (Kolkata, India), EIPICO (Cairo, Egypt), Honour lab limited (Mumbai, India) and AMOUN pharmaceuticals (Cairo, Egypt); respectively and were marked each with labels indicating purity of at least 98.5%. RDS's chemical structure as well as its related interferants are displayed in Fig. 1.

2.2.2. Pharmaceutical formulation

Remdesivir® IV injection (100 mg/20 mL per vial) was produced by EVA PHARMA Egypt (batch no. 2105598).

2.3. Chemicals and reagents

Analytical-grade chemicals and reagents were used throughout and water was bidistilled. Sigma Aldrich (Steinheim, Germany) provided sodium tetraphenylborate (NaTPB), graphene nanoplatelets, N-methylpyrrolidone (NMP) and polyvinyl pyrrolidone (PVP). Alfa Aesar (a Massachusetts company, Ward Hill, USA) provided Calix-8-arene, Tricresyl Phosphate, and Sodium Dodecyl Sulfate (SDS). Aniline came from Techno pharmchem (Delhi, India), while ammonium persulfate (APS) was purchased from Oxford Lab Fine Chem in Maharashtra, India. From Fluka (Steinheim, Germany), polyvinyl chloride (PVC) was produced. Merck (Darmstadt, Germany) provided tetrahydrofuran (THF) and dimethyl sulphoxide (DMSO). Xylene and Hydrochloric acid were purchased from Prolabo (Pennsylvania, USA). El-Nasr Company (Cairo, Egypt) provided potassium chloride and sodium hydroxide.

VACSERA (The Holding Company for Vaccines and Biological Products) in (Giza, Egypt) supplied human plasma samples, which were kept at a temperature of 4 °C.

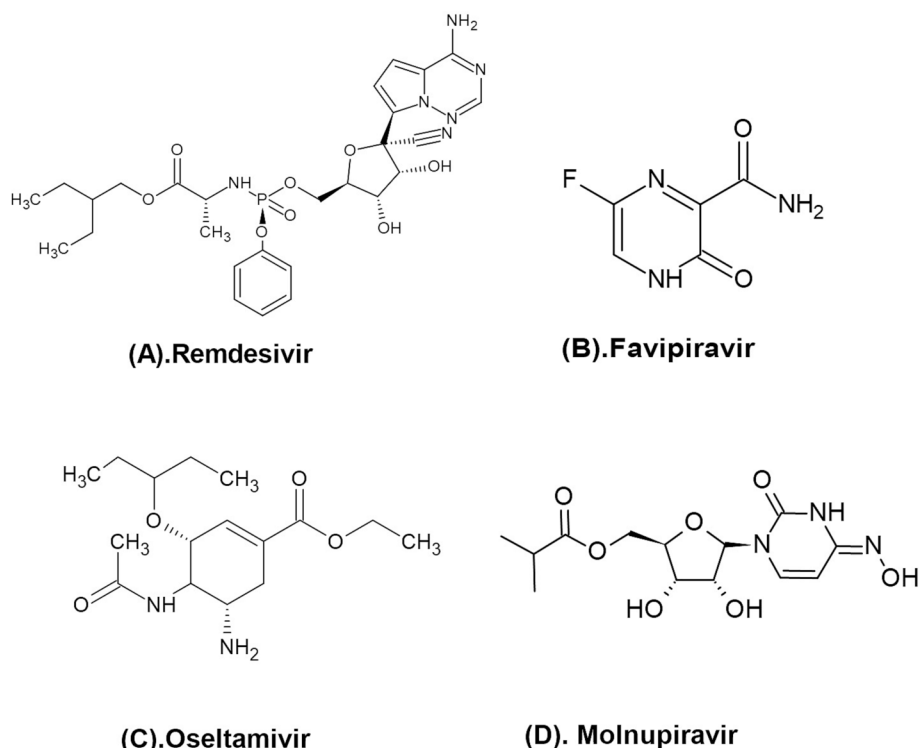


Fig. 1. Chemical structure of (A). Remdesivir and its interferants (B). Favipiravir, (C). Oseltamivir, (D). Molnupiravir.

2.4. Standard solutions

1×10^{-2} M RDS (standard solution) was obtained by dissolving 0.3 g in 20-mL methanol, sonication for 5 min and then completing to the desired volume (50-mL) using dil HCl (pH 3). A series of dilutions was carried out to provide several working solutions ranging from 1×10^{-8} to 1×10^{-2} M using the same dil HCl (pH 3) throughout the whole experiment.

2.5. Procedure

2.5.1. Preparation of graphene nanocomposite

10% (w/w) graphene nanocomposite was generated using the solution dispersion technique [30], which involved dispersing 10.0 mg of graphene in 1.0 mL of xylene followed by sonication for 5 min.

2.5.2. Preparation and characterization of a dispersion of polyaniline nanoparticles

A modified version of the process described by Moulton et al. [31] was utilized to prepare chemically polymerized PANI nanoparticle dispersion, where the surfactant employed was SDS rather than dodecyl benzene sulfonic acid. Polymerization took place at 20 °C in a thermostated bath. In a round-bottomed flask, 100.0 mL of water, SDS and aniline (1.3 M each) were added, and the solution was mechanically mixed for an hour. Dropwise addition of 1.3 mol/L APS was then applied to the milky white aniline/SDS solution (100 mL). After allowing the polymerization to continue for 2.5 h, a dark green dispersion was created.

By utilizing a dialysis membrane (12,000 molecular weight cut-off) from Sigma against deionized water over forty eight hours, the polymerized dispersion was purified. Then, to eliminate extra SDS, it was agitated for 10 min at 15,000 rpm and rinsed four times in water. The PANI nanoparticles were then mixed with (10% w/w) xylene and kept in a brown glass bottle that was tightly closed.

Using a UV-VIS spectrophotometer, characterization of PANI was conducted. The Malvern Zetasizer was used to measure Zeta potential in

order to determine PANI particle size.

2.5.3. Preparation of Graphene/PANI nanocomposite

The Graphene/PANI nanocomposite was prepared according to [32] by dissolving aniline monomer (1.0 g) in conc. HCl (1.0 mL) and then diluting it with distilled water till (10.0 mL) (solution I). The next step was to add 10 mg of graphene to solution I, then sonication for 2 h to create aniline-graphene dispersion. Using a different beaker, distilled water (90.0 mL) was used to dissolve conc. HCl (0.8 mL), APS (1.0 g) and PVP (2.0 g) to form (solution II). After that, solution II was allowed to cool for 30 min in iced water bath. To create a powder precipitate, solutions I and II were continually stirred vigorously for 4 h. Using nylon membrane filters (0.22 μ m), the precipitate was filtered and washed with ethanol and distilled water until the filtrate turned colorless, then dried (on the filter) for a whole night at 65 °C. The precipitate formed was re-dispersed in 0.1 M HCl while being ultrasonically agitated for 30 min, filtered once more, and dried to demonstrate that G/PANI was fully loaded with HCl [33]. The creation of Graphene/PANI nanocomposite is displayed in Fig. A1. IRS Spirit Fourier transform infrared spectrophotometer, (Serial no. A224156), Shimadzu Corp. (Kyoto, Japan) and High resolution scanning electron microscopy using a field emission gun (SEM Quanta FEG 250, FEI Company, Netherlands) were used to analyze the PANI and G/PANI nanocomposite modified electrode.

2.5.4. Fabrication of membrane sensors

In a glass Petri dish (5 cm diameter), NaTPB (0.01 g), calix-8-arene (0.05 g), TCP (0.4 g) and PVC (0.19 g) were combined to construct the ion selective membrane solution. 6 mL of THF was used to dissolve the mixture.

5 mm diameter graphite rods (15 mm length) were pushed inside polyethylene tubes. The ends of the rods underwent mechanical polishing, water washing, and air drying.

Graphene dispersion was poured on the top surface of a graphite rod and allowed to evaporate for 24 h in the air in order to fabricate (Sensor II). Drop casting was used to apply the 30 μ L ion selective membrane solution to the graphene layer.

For Sensor III, 10 μL of PANI dispersion was drop casted individually onto the top side of another graphite rod in order to fabricate the PANI sensor. Then 30 μL of the ion selective membrane solution was applied to cover the PANI layer where the solvent was left to evaporate for 24 h.

A blank sensor (Sensor I) was created by applying the ion selective membrane directly to the graphite sensor without adding ion to electron transducer layer for comparison with the other sensors.

N-methylpyrrolidone was used to disperse the G/PANI nanocomposite in accordance with the previously reported method [29]. For electrode modification using drop-casting, the working electrode was covered with 1.0 mL of the G/PANI dispersion. This coating was left overnight to completely dry at room temperature then the ion selective membrane solution (30 μL) was drop casted onto the G/PANI layer (Sensor IV).

The four sensors' ion selective membranes were then left to evaporate overnight. The sensors were preconditioned by submerging them in a 10^{-3} mol/L RDS solution for 24 h. When not in use, the sensors were kept in the same solution.

2.5.5. Potentiometric measurements and sensors calibration

By transferring aliquots of RDS solutions covering the range of (1×10^{-8} to 1×10^{-2} mol/L) sequentially into a set of 100-mL beakers, the conditioned sensors were calibrated. The potentials were measured while the reference electrode and proposed sensors were dipped in each solution and constantly stirred. Plots of the electrode potential versus RDS concentration in the negative logarithmic range were constructed. The linear portion of the curve's regression equation was calculated.

2.5.6. Potentiometric determination of RDS in IV injections

50-mL volumetric flasks were filled with a volume (1.00 mL) of RDS IV injection (100 mg/20-mL vial) equivalent to 5 mg RDS and completed with dil HCl to obtain final concentration of 0.10 mg/mL. From this solution, 30.00 mL were extracted and completed to the final volume (50.00 mL) using dil HCl (pH = 3) to obtain the calibration concentration 1.00×10^{-4} mol/L. Other samples were prepared in the same manner and had final concentrations of 1.00×10^{-6} , 1.00×10^{-5} and 1.00×10^{-4} mol/L. With the suggested sensors, the potentiometric measurements were carried out.

2.5.7. Potentiometric determination of RDS in spiked human Plasma

A falcon tube containing 0.50 mL of RDS-free human plasma was filled, spiked with aliquots of RDS working standard solutions, and then vortexed for 5 min. The plasma proteins were then precipitated by adding two mL of acetonitrile, mixing for an additional five minutes, and centrifuging for 20 min at 6000 rpm. The supernatant was collected in 10-mL volumetric flasks where the volumes were filled to the mark using HCl (pH = 3) to provide final RDS concentrations of 0.50×10^{-6} , 1.00×10^{-6} , 0.50×10^{-5} and 1.00×10^{-5} mol/L. The resultant potentials were noted, and using the associated regression equations, the relevant concentrations were determined.

3. Results and discussion

The aim of this work is to investigate and compare different ion selective SC electrodes for the measurement of the drug's active ingredient (RDS) in human plasma. The ionophore CX8 was selected for the RDS-selective sensor because it has exceptional complexation capabilities for organic ammonium ions. The interaction of RDS and tetraphenyl borate inside CX8 ionophore was used as the sensing element in all of the studied electrodes. The very hydrophobic PANI nanoparticles were utilized as an ion-to-electron transducer in SC electrodes to serve as a suitable intermediary layer between an ion-selective membrane and the solid contact in an attempt to improve the electrode stability and limit water uptake. Graphene nanoplatelets were also employed with enhanced reproducibility. A third electrode used a composite material made of both graphene nanoplatelets and electrically conductive PANI

as the ion-to-electron transducer. Graphene and electroactive conducting polymers act together synergistically in this concept, increasing the electrocatalytic activity at the electrode substrate/SC interface. These nanoparticles were chemically produced and analyzed. This ought to provide a strong foundation for sensor development for pharmaceutical analysis.

3.1. Characterization of PANI nanoparticles and G-/PANI nanocomposite

3.1.1. Scanning electron Microscope (SEM)

SEM was used to examine the surface morphological characteristics of fabricated PANI nanoparticles and G/PANI nanocomposite (Figs. 2A, 2B). The aniline monomer solution was enriched with 10 mg of graphene to increase the electroactivity and conductivity of PANI nanoparticles. The G/PANI composite particles were somewhat more uniformly distributed than PANI nanoparticles, as shown in Fig. 2B.

3.1.2. Fourier transform infrared spectroscopy (FTIR)

FTIR was used to further characterize the particles (Fig. A2). In order to identify different functional groups in the samples, the FTIR spectra of PANI, graphene nanoplatelets and G/PANI composite were generated. Fig. A2(A) depicts the FTIR spectrum of pure graphene, which is devoid of any peaks. The FTIR spectrum of PANI exhibits distinctive peaks for different stretching and bending vibrational modes connected with its chemical structure Fig. A2(B). The N-H stretching was shown by a peak in PANI at 3440 cm^{-1} . The C=C and C-C stretching of the quinoid and benzenoid rings; respectively, were attributed to the bands at 1489.95 cm^{-1} and 1462.83 cm^{-1} . The N-H bend for primary amines was shown by a band at 1650 cm^{-1} . At 1288.72 cm^{-1} , the band corresponding to the benzenoid and quinoid rings' C-N stretching was discovered. In addition to these bands, PANI salt exhibits bands at 2900 and 2800 cm^{-1} linked to symmetrical and asymmetrical stretching of the dodecyl hydrogen sulphate alkyl substituent utilized in the polymerization step. Although the spectra of G/PANI Fig. A2(C) showed absolutely similar vibrational bands to pure PANI, the slight variations from the recognizable bands at 3200 cm^{-1} , 1494.23 cm^{-1} , 1400.04 cm^{-1} , 1215.94 cm^{-1} and C=C stretching band at 1600 cm^{-1} can be justified by molecular interactions between PANI and graphene. At 820.61 cm^{-1} , 743.55 cm^{-1} and 619.39 cm^{-1} , C-H bending vibrations could be seen. These results proved that graphene and PANI combined to create a composite particle. These outcomes are in agreement with [34,35].

3.1.3. Dynamic light scattering (DLS) characterization

By using dynamic light scattering (DLS), the average hydrodynamic sizes of the chemically produced PANI and G/PANI NPs were determined to be 147.4 & 281.3 nm respectively (Fig. A3).

3.1.4. UV/VIS characterization of PANI and G/PANI nanocomposite

Fig. 3 displays the UV-visible spectra of the PANI, PANI in alkaline medium as well as G/PANI nanoparticles. The PANI spectrum shows an absorption band at 280 nm that corresponds to $\pi-\pi^*$ benzenoid ring electronic transitions of the PANI emeraldine salt form. The production of polarons and bipolarons in PANI's macromolecular chain is also indicated by the presence of a shoulder band at 425 nm and a growing absorption band at 835 nm. The PANI nanoparticles, however, were transformed into the insulating emeraldine base form in an alkaline pH, as seen by their distinctive absorption spectrum. These findings show that PANI nanoparticles are sensitive to pH changes. The G/PANI nanocomposite exhibits the same pattern of peaks as emeraldine PANI but with minor positional changes. The $\pi-\pi^*$ excited state peak has been seen in the G/PANI at 330 nm with a 50 nm blue shift. The absorption peak associated with polaron production, on the other hand, emerges at 435 nm with a blue shift of 10 nm. The interaction of the protonated form of polyaniline with the aromatic rings in graphene sheets may be responsible for the observed shifts in wavelengths. Beyond 490 nm, an

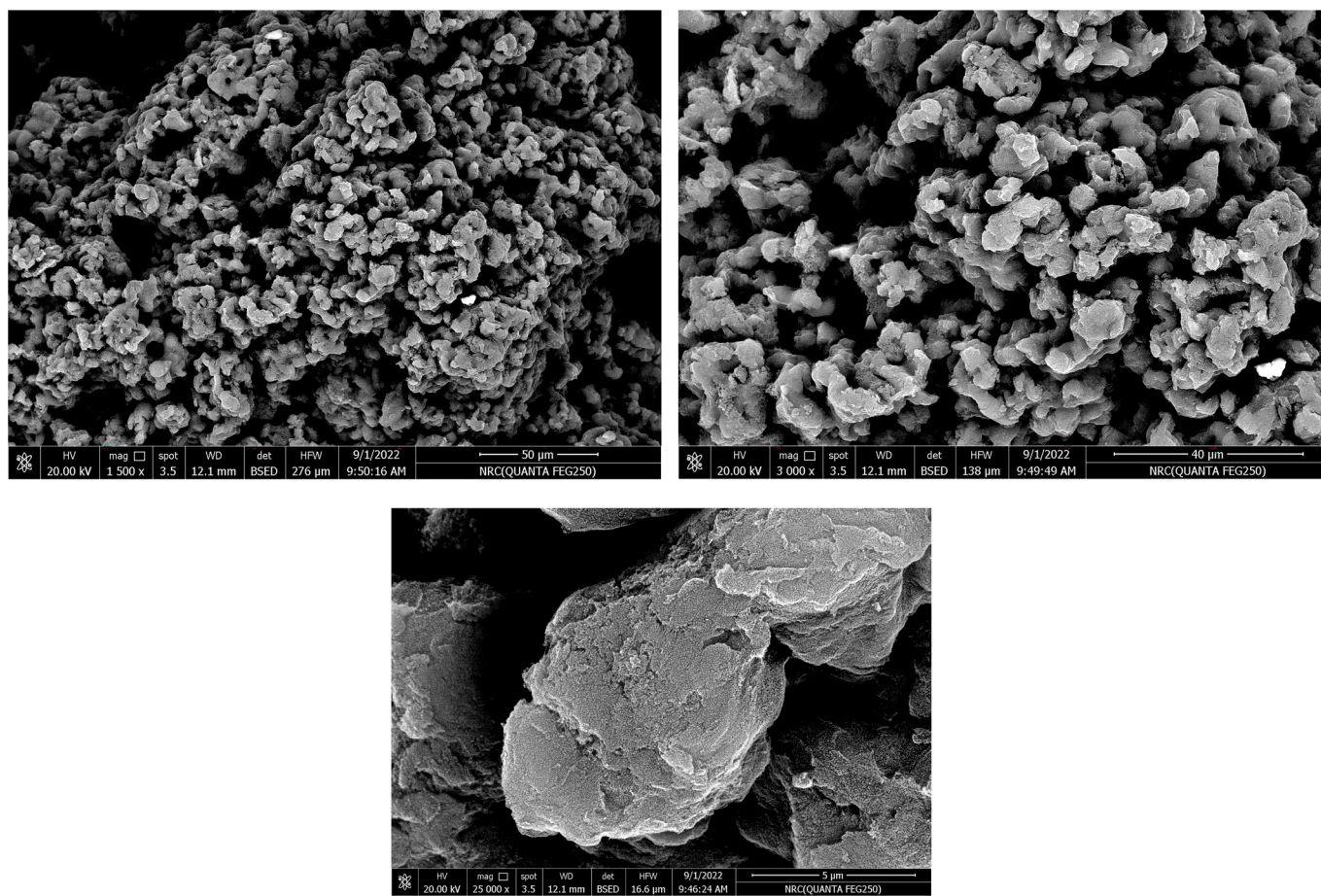


Fig. 2A. SEM images of PANI nanoparticles.

increasing absorption edge consistent with the production of bi-polarons was also noted for the G/PANI nanocomposite. Our findings were consistent with those found in the literature [36,37].

3.2. Performance characteristics of Graphene, PANI nanoparticles and G/PANI nanocomposite based SC/ISEs

It seems that generating SC-ISEs with reliable standard potentials remains a serious issue despite the considerable work in this field. In this study, the performance of the sensors employed (Sensors II, III & IV) based on Graphene, PANI NPs and G/PANI was assessed in comparison to a blank sensor (Sensor I) which was devoid of an ion to electron transducer layer. According to the IUPAC requirements [38], the electrochemical performance parameters of the four suggested sensors were assessed and are listed in Table 1.

The composition and constituent elements of the membrane have a major impact on the response properties of ion-selective electrodes. We investigated the impact of different modifiers; Graphene, PANI and G/PANI in order to assess the influence of membrane on electrode responses. RDS has a tertiary amine group attached to the phosphate group that acts as a cation in acidic conditions. Tetraphenylborate was added to the RDS-ISM as a cation exchanger for the formation of 1:1 association complex. This ratio was supported by the proposed electrodes' near-Nernstian response, which was roughly 60 mV/decade—a typical slope for monovalent drugs.

For sensors (I, II, III & IV), the calibration plots showed slopes of 49.61, 49.53, 51.18, and 55.39 mV/concentration decades; respectively (Fig. 4). Both sensors I and II exhibited near Nernstian responses. However, better Nernstian slopes were obtained for sensors III & IV. As shown in Table 1, Sensor II demonstrated greater sensitivity over a

broad concentration range from 10^{-7} to 10^{-2} mol/L. Sensors IV was capable of measuring concentrations between 10^{-7} to 10^{-3} mol/L. While for Sensors I & III, concentration ranges were between 10^{-6} and 10^{-2} mol/L. Limits of detection were calculated from the intersection of the two extrapolated segments of the calibration graph as shown in Table 1 where sensors II & IV containing graphene showed lower detection limits than other sensors. The incorporation of graphene nanoplatelets increased the electrical signal's stability and reduced the possibility of potential drift because of the increased specific surface area that increased the electrode double layer capacitance. That's why sensors I and III had shorter life spans (30 and 50 days; respectively) than sensors II & IV.

Taking in consideration all of the above, sensor IV demonstrated superior performance in terms of slope, sensitivity, accuracy and durability, while sensor II demonstrated the best performance in terms of sensitivity and precision. Table 1 lists every performance criterion for the suggested sensors, including linearity ranges, accuracy and precision.

3.3. Dynamic response time

To maximize the quantity of samples evaluated over a short period of time, dynamic response time is a crucial factor. For sensors I, II, III and IV, the reaction times in samples were 25, 10, 15, and 7 s; respectively. This indicates that the electrochemical system attains equilibrium much faster with sensor IV than with the other sensors. This may be explained by the high capacitance and enormous surface areas of the conducting polymer nanoparticles, which result in short response times and rapid charge transfer rates. As the activity of ions increases, the time needed for the electrochemical system to attain equilibrium becomes shorter,

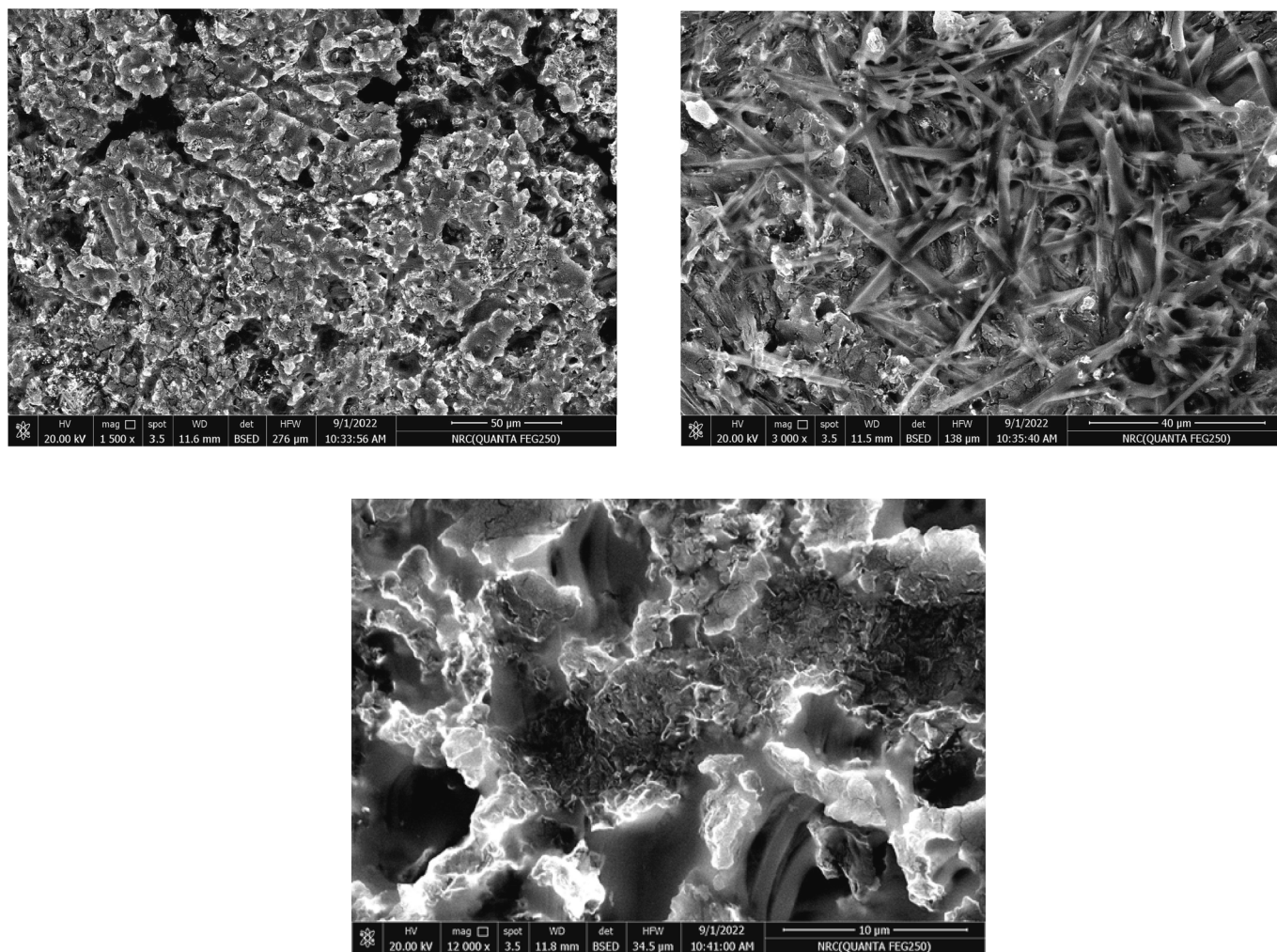


Fig. 2B. SEM images of G/PANI nanocomposite.

and the response time becomes smaller. The average response time with standard deviation (SD) for each sensor is shown in Table 1.

Using a 10^{-4} mol/L RDS solution, EMV was measured for 5 h to estimate the intermediate potential stability. For sensors III and IV, small drift measurements of 1.2 and 0.7 mV h^{-1} ; respectively, were observed. The drift on Sensor II was higher, at 2.9 mV h^{-1} . While sensor I recorded the greatest drift (18.4 mV h^{-1}). These findings are consistent with those of graphene-based SC sensors [39], PANI NPs-based sensors [40] and G/PANI based sensors [27] that were previously published.

Daily calibration was used to evaluate the proposed electrodes' lifetime. The proposed sensors' life times (long potential stability) were discovered to be 30, 60, 50 and 60 days without any notable changes; respectively, for sensors I, II, III and IV.

Water layer growth between the ion selective membrane and the solid contact may be the cause of the blank sensor's shorter lifespan, increased potential drift and longer response time. Potentiometric water layer testing was done to assess this.

3.4. Potentiometric water layer test

In some solid contact ion selective electrodes (SC-ISEs), the creation of an aqueous film (or "water layer") between the ion-selective membrane and its solid contact may be partially responsible for the drifting potentials and the poor potential repeatability and reproducibility [41]. The "water layer test" procedure has been a standard procedure for evaluating the performance traits of SC-ISEs.

This test is used to identify the presence of a water layer between the ion-to-electron transducer layer and the ion sensing membrane. It relies on identifying potential drift when a SC electrode that has reached full equilibrium in a main ion solution (RDS; 10^{-4} M) is then exposed to a solution that solely contains competing ions (FAV; 10^{-2} M), and the electrode potential is recognized until the new equilibrium is reached. The electrode is then returned to the primary ion solution, and its potential is once more recorded until the initial equilibrium is reached.

When the solution's composition abruptly changes (for instance, when it goes from RDS to FAV and back to RDS), the electrode potential immediately steps up. This occurs with SC electrodes devoid of a water layer because the electrode potential depends on the selectivity coefficient and the concentration change. However, for non-ideal SC electrode behavior that has a water layer between the SC and the ion-selective membrane, the electrode potential gradually drifts in a different direction to the potential before the step-change in the solution composition.

Fig. 5 demonstrates that in sensors III and IV, the response to the principal ion is the same (same potential) both prior to and following exposure to the competing ion. This driftless potential response shows that there is no aqueous layer at the contact between the ion sensing membrane with each of PANI and G/PANI. The large potential drift as depicted in Fig. 5 occurred due to the absence of an ion-to-electron transducer layer in sensor I. Instead, a water layer was formed beneath the membrane. In addition, sensor II also suffered a very small drift at 6 hr, however, this drift was eliminated by adding polyaniline layer in sensor IV.

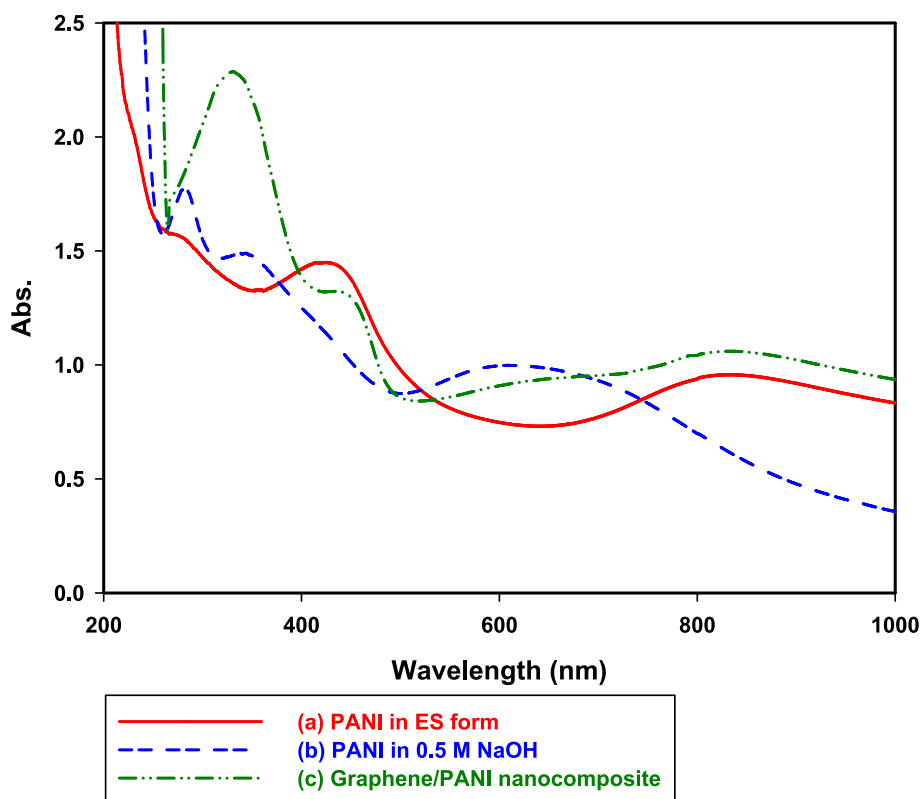


Fig. 3. UV-VIS characterization of (a) PANI in the ES form, (b) after dedoping to the EB form using 0.5 M NaOH, (c) PANI/Graphene nanocomposite.

Table 1
Performance characteristics of RDS Solid Contact sensors.

Parameter	Sensor 1	Sensor 2	Sensor 3	Sensor 4
Slope (mV/decade)	49.61 ±	49.53 ±	51.18 ±	55.39 ±
± SD ^a	3.80	3.60	1.40	0.50
Intercept	474.50	588.59	495.42	467.05
Linear range (mol/L)	10 ⁻⁶ -10 ⁻²	10 ⁻⁷ -10 ⁻²	10 ⁻⁶ -10 ⁻²	10 ⁻⁷ -10 ⁻³
Correlation Coefficient (r)	0.9977	0.9989	0.9980	0.9993
LOD (mol/L)	1.00 × 10 ⁻⁶	1.00 × 10 ⁻⁷	1.00 × 10 ⁻⁶	1.00 × 10 ⁻⁷
Response time (sec.)	25 ± 4	10 ± 2	15 ± 3	7 ± 1
Stability (days)	30	60	50	60
Working pH range	2-4	2-4	2-4	2-4
Accuracy ^b (%) ±	100.22 ±	100.18 ±	100.92 ±	100.03 ±
SD	2.20	1.47	2.71	1.09
Repeatability (%R.S.D)	1.94	1.21	3.02	2.85
Intermediate precision (%R.S.D)	1.61	0.46	1.58	1.31

^a Standard deviation.

^b Assessed by recovery rates of standard samples.

Ion fluxes and atmospheric gas diffusion are caused by the creation of an aqueous layer underneath the membrane causing changes in ionic composition of the ion sensing membrane and the characteristic potential drifts. Each modification in the composition of the sample necessitates a re-equilibration of the water layer that serves as an ionic reservoir, which in turn lengthens the response time. Additionally, the aqueous layer causes the membrane to rapidly detach from the solid contact. As a result, the sensor's lifespan is drastically reduced [42] as shown by 30 days lifetime for sensor I.

Neither PANI nor G/PANI can produce a water film because of their extreme hydrophobicity. Additionally, they have a remarkable quality that allows for a reversible change from ionic to electronic conductivity,

and they have a large capacitance, which provides the possibility of stability.

3.5. Effect of pH

With the aid of Britton Robinson buffer and 10⁻⁴ M RDS, the impact of pH on the potential response of the sensors under investigation was explored over a range of pH 2 to 10. As illustrated in Fig. A4, the four proposed sensors displayed steady potentials between pH 2 and 4. As a result, this range was selected for the suggested sensors in order to function. It was shown that the potentials decrease above pH 4, which may be related to RDS's instability at alkaline pH [43].

RDS has a pka of 3.56 and at pH 2, the majority of RDS has a positive charge [44]. Due to the low aqueous solubility of RDS, standards were prepared in HCl acidic solutions adjusted at pH (3) to increase the drug's solubility as well as to prolong the sensors' lifetime.

3.6. Sensors selectivity

Using the matched potential method (MPM) [45], the potential coefficients of selectivity ($K_{pot A, B}$) of the suggested sensors were assessed for related pharmaceuticals like Favipiravir, Molnupiravir and Oseltamivir, and inorganic ions like potassium and sodium chloride.

The IUPAC-recommended MPM [46] has a wide range of applications for ions with different charges, including non-Nernstian interfering ions. Thus, using MPM enables the production of unbiased more meaningful results than those obtained using the separate solution approach [45].

A selectivity coefficient of 1.0 means that the membrane reacts to primary and interfering ions equally. The electrode is said to be selective to primary ion over interfering ion if the value is less than 1.0, which suggests that it responds more to primary ions than interfering ions. Table 2 as well as Fig. A5 demonstrate the selectivity coefficients of the suggested sensors which selectively respond to the drug under

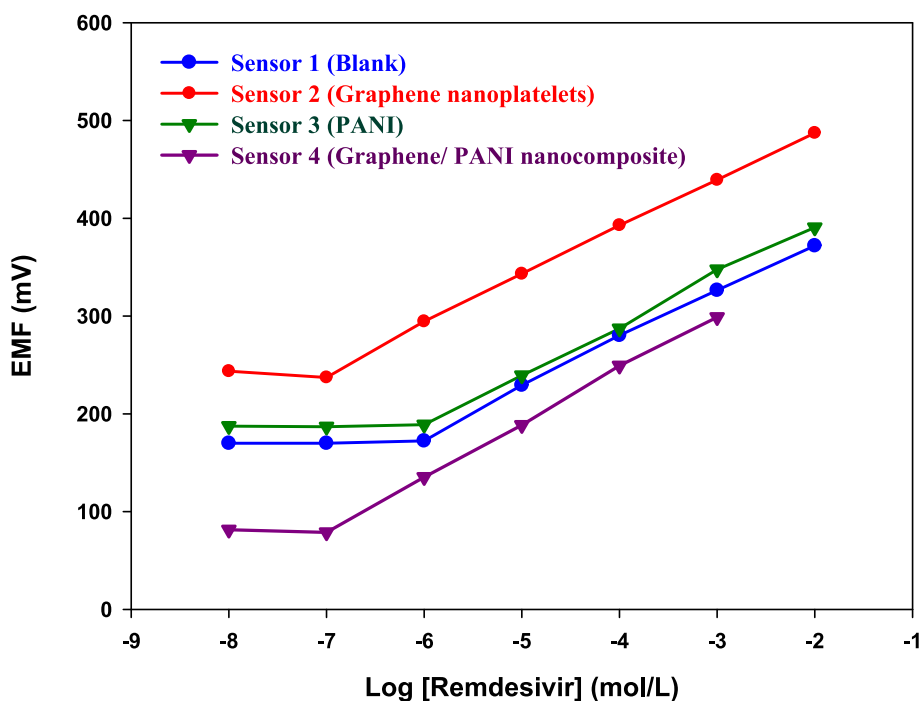


Fig. 4. Profile of the potential (mV) versus -log concentrations of RDS (mol/L) of the proposed sensors.

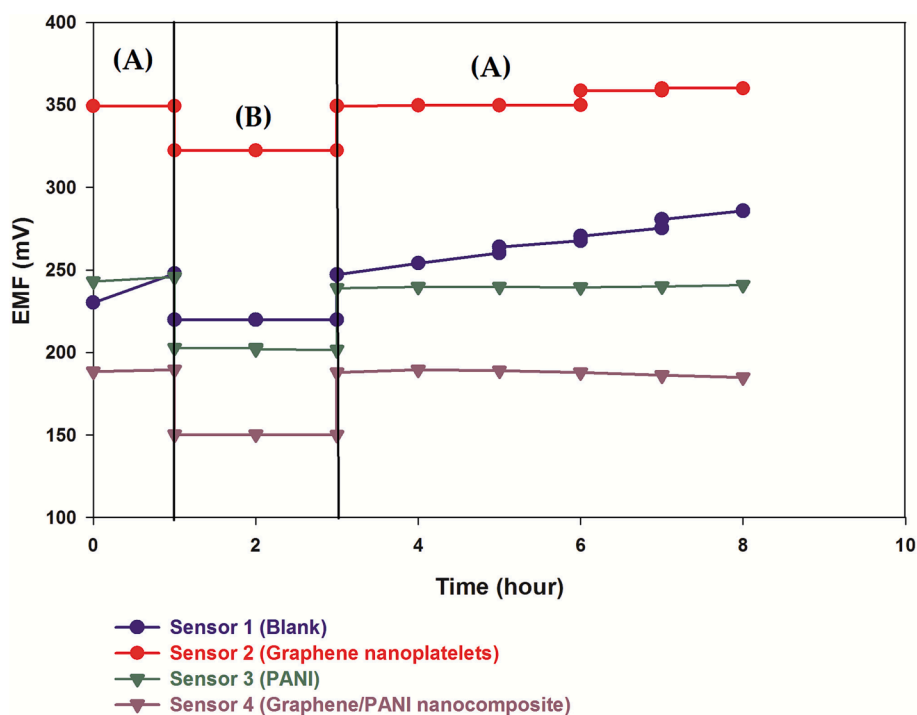


Fig. 5. Potentiometric water layer test. EMF was recorded successively in (A) 10^{-4} mol/L RDS, then (B) 10^{-2} mol/L Favipiravir and back to (A) 10^{-4} mol/L RDS by the proposed sensors.

investigation. The findings suggest that all of the sensors exhibit reasonable selectivity. Sensors III & IV display the greatest selectivity and the least response to potentially interfering compounds owing to their lower selectivity coefficients compared to sensors I & II. As a result, both sensors are thought to be the best for detecting RDS in the presence of other interfering compounds.

It is also obvious that Oseltamivir displays relatively higher selectivity coefficient. This may be due to the fact that Oseltamivir has similar

structural characteristics to RDS such as valency, solubility and lipophilicity where Oseltamivir is monovalent ($n = 1$) due to $-NH$ group which is connected to CO [47] similar to RDS which has a phosphate attached to $-NH$ group as shown in Fig. 1. The partition coefficient (Log P) between octanol and water is commonly used as measure of lipophilicity. Log p for Oseltamivir is 1.1 [48], while for RDS is 3.2 [49]. Thus, both have low water solubility. In contrast, the ionic size, solubility and lipophilicity of Favipiravir (Log P = -0.49) [50] and

Table 2

Potentiometric selectivity coefficients ($K_{pot}^{RDS, \text{interferent}}$)^{*} for the investigated solid contact sensors.

Interferant	Sensor 1	Sensor 2	Sensor 3	Sensor 4
Favipiravir	1.8×10^{-2}	9.0×10^{-2}	8.0×10^{-3}	1.8×10^{-2}
Oseltamivir	4.9×10^{-1}	4.9×10^{-1}	1.9×10^{-1}	1.9×10^{-1}
Molnupiravir	9.0×10^{-2}	4.0×10^{-2}	4.0×10^{-3}	4.0×10^{-3}
NaCl	4.0×10^{-3}	4.0×10^{-3}	4.0×10^{-3}	4.0×10^{-3}
KCl	4.0×10^{-3}	4.0×10^{-3}	4.0×10^{-3}	4.0×10^{-3}

^{*} $K_{pot}^{A,B} = \Delta aA/aB$, with $\Delta aA = a'_{A} - a_A$, where $K_{pot}^{A,B}$ denotes the selectivity coefficient, ion A is the primary ion, ion B is the interfering ion and a_A is the initial background activity of ion A.

Molnupiravir (Log P = -0.8) [51] compared to RDS ions is primarily responsible for the strong selectivity against these compounds as they are more water soluble and less lipophilic in addition to their low molecular weights. Also, inorganic cations as sodium and potassium did not interfere due to the variations in their ionic size, mobility, and permeability when compared to the RDS ions.

3.7. Potentiometric determination of RDS in IV injections and human Plasma

Remdesivir's maximum concentration in the human plasma reaches 3 $\mu\text{mol/L}$ [52]. Thus, a sensitive, selective and reliable method is required for its quantitation. The suggested sensors were successfully employed for the assessment of RDS in Remdesivir® IV injections as well as spiked human plasma where they proved to be successful in obtaining precise and reliable recoveries without tedious sample pretreatment. However, best recoveries in human plasma were obtained using sensor IV as illustrated in Table 3.

4. Conclusions

Four ion selective electrodes have been developed for the estimation of the anti-COVID-19 medication RDS. Excellent potentiometric analytical performance, highest sensitivity and low cost were all displayed by the graphene-based electrode, which was also simple to fabricate. High selectivity and excellent reproducibility were obtained using the PANI/solid contact sensor system. In order to obtain a sensitive and selective detection, we have employed a composite material made of graphene nanoplatelets and electrically conductive PANI. Graphene's inclusion has further enhanced response properties and potential stability owing to the electrocatalytic action of the G/PANI composite, which speeds up electron transfer at the substrate/transducer interface. It also increased the reliability of the response in conjunction with its enhanced hydrophobicity. Having a slope of 55.39 ± 0.5 mV/decade, an LOD of 100 nmol/L and strong potential response stability, the ISE using G/PANI as the transducer was the best sensor for Remdesivir determination in comparison to the coated graphene ISE or the neat PANI transducer.

Funding

No funding was received to assist with the preparation of this manuscript.

CRediT authorship contribution statement

Noha F. El Azab: Conceptualization, Methodology, Formal analysis, Investigation, Writing – original draft, Writing – review & editing, Supervision. **Neven Ahmed:** Writing – original draft, Resources.

Declaration of Competing Interest

The authors declare that they have no known competing financial

Table 3

Determination of RDS in Remdesivir® IV Injection (100 mg/20-mL vial) and spiked human plasma using the proposed Solid Contact sensors.

Matrix	Claimed concentration ($\mu\text{mol/L}$)	Recovery \pm SD ^a			
		Sensor 1	Sensor 2	Sensor 3	Sensor 4
Remdesivir® IV Injection	1.00	105.56 \pm 1.38	101.51 \pm 2.02	103.51 \pm 0.73	103.02 \pm 0.62
	10.00	103.62 \pm 1.56	101.36 \pm 1.89	103.62 \pm 0.69	96.21 \pm 0.59
	100.00	104.83 \pm 1.21	105.40 \pm 1.94	104.83 \pm 0.71	99.36 \pm 0.61
Human plasma	0.50	96.43 \pm 2.01	93.56 \pm 2.24	91.18 \pm 1.27	103.67 \pm 0.45
	1.00	92.72 \pm 1.78	91.66 \pm 1.66	95.54 \pm 0.91	94.46 \pm 0.36
	5.00	91.65 \pm 1.84	93.89 \pm 1.52	93.77 \pm 0.89	93.15 \pm 0.42
	10.00	90.01 \pm 0.89	95.42 \pm 1.55	91.02 \pm 0.85	95.71 \pm 0.24

^a Average of 3 determinations.

interests or personal relationships that could have appeared to influence the work reported in this paper.

Data availability

Data will be made available on request.

Acknowledgements

We have not included an Acknowledgement, that indicates that we have not received substantial contributions from non-authors.

Appendix A. Supplementary data

Supplementary data to this article can be found online at <https://doi.org/10.1016/j.microc.2023.108658>.

References

- [1] G.J. Kontoghiorghes, S. Fetta, C.N. Kontoghiorghes, The need for a multi-level drug targeting strategy to curb the COVID-19 pandemic, *Front. Biosci.-Landmark* 26 (2021) 1723–1736.
- [2] A. Chera, A. Tanca, Remdesivir: the first FDA-approved anti-COVID-19 treatment for young children, *Discoveries* 10 (2022).
- [3] R. Nguyen, J.C. Goodell, P.S. Shankarappa, S. Zimmerman, T. Yin, C.J. Peer, W. D. Figg, Development and validation of a simple, selective, and sensitive LC-MS/MS assay for the quantification of remdesivir in human plasma, *J. Chromatogr. B* 1171 (2021), 122641.
- [4] I. Bulduk, E. Akbel, A comparative study of HPLC and UV spectrophotometric methods for remdesivir quantification in pharmaceutical formulations, *J. Taibah Univ. Sci.* 15 (2021) 507–513.
- [5] D.A.M. Noureldeen, J.M. Boushra, A.S. Lashien, A.F.A. Hakiem, T.Z. Attia, Novel environment friendly TLC-densitometric method for the determination of anti-coronavirus drugs "Remdesivir and Favipiravir": green assessment with application to pharmaceutical formulations and human plasma, *Microchem. J.* 174 (2022), 107101.
- [6] N.F. El Azab, A validated UHPLC-MS/MS method for simultaneous quantification of some repurposed COVID-19 drugs in rat plasma: application to a pharmacokinetic study, *Microchem. J.* 178 (2022), 107321.
- [7] H. Elmansi, A. Ehab, I. Mikhail, F. Belal, Green and sensitive spectrofluorimetric determination of Remdesivir, an FDA approved SARS-CoV-2 candidate antiviral; Application in pharmaceutical dosage forms and spiked human plasma, *Analyt. Methods* 13 (2021).
- [8] M. Rizk, M.A. Sultan, B.M. Tawfik, R.T. El-Eryan, Highly sensitive and selective sensing probe for determination of anti-Covid-19 Remdesivir: application to pharmaceutical dosage form and biological fluids, *J. Electrochem. Soc.* 169 (2022), 026522.
- [9] F.M. Abdel-Gawad, Y.M. Issa, M.E.M. Hassouna, E.M. Hussien, Piribedil-selective electrodes based on Bi(III)-Iodide and Hg(II)-Iodide complexes, *Microchim. Acta* 141 (2003) 7–13.
- [10] M.F. Abdel-Ghany, L.A. Hussein, N.F. El Azab, Novel potentiometric sensors for the determination of the dinotefuran insecticide residue levels in cucumber and soil samples, *Talanta* 164 (2017) 518–528.

- [11] N.F. El Azab, A.M. Mahmoud, Y.A. Trabik, Point-of-care diagnostics for therapeutic monitoring of levofloxacin in human plasma utilizing electrochemical sensor mussel-inspired molecularly imprinted copolymer, *J. Electroanal. Chem.* (2022) 116504.
- [12] S. Ryasenskii, M. Feofanova, D. Vasil'eva, G. Mantrov, Solid-state ion-selective electrode with an ion-electron transducer for doxycycline determination, *Pharm. Chem. J.* 50 (2016) 205–208.
- [13] F. Kazemi, S.M. Naghib, Y. Zare, K.Y. Rhee, Biosensing applications of Polyaniline (PANI)-based nanocomposites: a review, *Polym. Rev.* 61 (2021) 553–597.
- [14] M. Sorvin, S. Belyakova, I. Stoikov, R. Shamagsumova, G. Evtugyn, Solid-contact potentiometric sensors and multisensors based on polyaniline and thiacalixarene receptors for the analysis of some beverages and alcoholic drinks, *Front. Chem.* 6 (2018) 134.
- [15] M.R. Elghobashy, A.M. Mahmoud, M.R. Rezk, M.K. Abd El-Rahman, Strategy for fabrication of stable tramadol solid-contact ion-selective potentiometric sensor based on polyaniline nanoparticles, *J. Electrochem. Soc.* 162 (2014) H1.
- [16] K. Milakin, A. Korovin, E. Moroz, K. Levon, A. Guiseppi-Elie, V. Sergeyev, Polyaniline-based sensor material for potentiometric determination of ascorbic acid, *Electroanalysis* 25 (2013) 1323–1330.
- [17] E. Kulapina, M. Tyutlikova, O. Kulapina, A. Dubasova, Solid-contact potentiometric sensors for the determination of some cephalosporin antibiotics in pharmaceuticals and oral fluid, *J. Anal. Chem.* 74 (2019) 52–58.
- [18] T.V. Shishkanova, K. Videnská, S.G. Antonova, M. Kronďák, P. Fitl, D. Kopecký, M. Vrnáta, V. Král, Application of polyaniline for potentiometric recognition of salicylate and its analogues, *Electrochim. Acta* 115 (2014) 553–558.
- [19] L.A. Hussein, N. Magdy, H.Z. Yamani, Stable glycopyrrolone bromide solid contact ion selective potentiometric sensors using multi-walled carbon nanotubes, polyaniline nanoparticles and polyaniline microparticles as ion-to-electron transducers: a comparative study, *Sens. Actuators B* 247 (2017) 436–444.
- [20] A. Parshina, A. Yelnikova, T. Titova, T. Kolganova, P. Yurova, I. Stenina, O. Bobreshova, A. Yaroslavl'tsev, Multisensory systems based on perfluorosulfonic acid membranes modified with polyaniline and PEDOT for multicomponent analysis of sulfacetamide pharmaceuticals, *Polymers* 14 (2022) 2545.
- [21] T.V. Shishkanova, A. Rezáčová, V. Král, N.P. Gospodinova, Influence of polyaniline on the potentiometric determination of risedronate with ion-selective membranes, *Anal. Methods* 2 (2010) 1614–1617.
- [22] D. Yuan, A.H. Anthis, M. Ghahraman Afshar, N. Pankratova, M. Cuartero, G. A. Crespo, E. Bakker, All-solid-state potentiometric sensors with a multiwalled carbon nanotube inner transducing layer for anion detection in environmental samples, *Anal. Chem.* 87 (2015) 8640–8645.
- [23] M.M. Khalil, W.M. El Roubay, I.H. Abd-Elgawad, Novel potentiometric sensors based on multiwalled carbon nanotubes and β -cyclodextrin for determination of antipsychotic sulpiride: electrochemical and surface morphology studies, *IEEE Sens. J.* 18 (2018) 3509–3516.
- [24] S.S. El-Mosallamy, K. Ahmed, H.G. Daabees, W. Talaat, A microfabricated potentiometric sensor for metoclopramide determination utilizing a graphene nanocomposite transducer layer, *Anal. Bioanal. Chem.* 412 (2020) 7505–7514.
- [25] M. Ganjali, F. Faridbod, N. Davarkhah, S. Shahtaheri, P. Norouzi, All solid state graphene based potentiometric sensors for monitoring of mercury ions in waste water samples, *Int. J. Environ. Res.* 9 (2015) 333–340.
- [26] E.Y. Frag, M.E. Mohamed, A.E. Ali, G.G. Mohamed, Potentiometric sensors selective for Cu (II) determination in real water samples and biological fluids based on graphene and multi-walled carbon nanotubes modified graphite electrodes, (2020).
- [27] Z.A. Boeva, T. Lindfors, Few-layer graphene and polyaniline composite as ion-to-electron transducer in silicone rubber solid-contact ion-selective electrodes, *Sens. Actuators B* 224 (2016) 624–631.
- [28] H. Gómez, M.K. Ram, F. Alvi, P. Villalba, E.L. Stefanakos, A. Kumar, Graphene-conducting polymer nanocomposite as novel electrode for supercapacitors, *J. Power Sources* 196 (2011) 4102–4108.
- [29] Z.A. Boeva, K.A. Milakin, M. Pesonen, A.N. Ozerin, V.G. Sergeyev, T. Lindfors, Dispersible composites of exfoliated graphite and polyaniline with improved electrochemical behaviour for solid-state chemical sensor applications, *RSC Adv.* 4 (2014) 46340–46350.
- [30] X. Li, Y. Xiao, A. Bergeret, M. Longerey, J. Che, Preparation of polylactide/graphene composites from liquid-phase exfoliated graphite sheets, *Polym. Compos.* 35 (2014) 396–403.
- [31] S.E. Moulton, P. Innis, L. Kane-Maguire, O. Ngamna, G.G. Wallace, Polymerisation and characterisation of conducting polyaniline nanoparticle dispersions, *Curr. Appl. Phys.* 4 (2004) 402–406.
- [32] N. Ruecha, N. Rodthongkum, D.M. Cate, J. Volckens, O. Chailapakul, C.S. Henry, Sensitive electrochemical sensor using a graphene–polyaniline nanocomposite for simultaneous detection of Zn (II), Cd (II), and Pb (II), *Anal. Chim. Acta* 874 (2015) 40–48.
- [33] P. Zhang, X. Han, L. Kang, R. Qiang, W. Liu, Y. Du, Synthesis and characterization of polyaniline nanoparticles with enhanced microwave absorption, *RSC Adv.* 3 (2013) 12694–12701.
- [34] H. Wang, Q. Hao, X. Yang, L. Lu, X. Wang, A nanostructured graphene/polyaniline hybrid material for supercapacitors, *Nanoscale* 2 (2010) 2164–2170.
- [35] X.M. Feng, R.M. Li, Y.W. Ma, R.F. Chen, N.E. Shi, Q.L. Fan, W. Huang, One-step electrochemical synthesis of graphene/polyaniline composite film and its applications, *Adv. Funct. Mater.* 21 (2011) 2989–2996.
- [36] N. Chen, Y. Ren, P. Kong, L. Tan, H. Feng, Y. Luo, In situ one-pot preparation of reduced graphene oxide/polyaniline composite for high-performance electrochemical capacitors, *Appl. Surf. Sci.* 392 (2017) 71–79.
- [37] S. Goswami, S. Nandy, T.R. Calmeiro, R. Igreja, R. Martins, E. Fortunato, Stress induced mechano-electrical writing-reading of polymer film powered by contact electrification mechanism, *Sci. Rep.* 6 (2016) 1–10.
- [38] A. Iup, Analytical chemistry division, commission on Ana-lytica I nomenclature, potentiometric selectivity coefficient of ion-selective electrodes, *Pure Appl. Chem.* 72 (2000) 1852.
- [39] S. Wang, L. Zhong, S. Gan, Y. Tang, S. Qiu, Y. Lyu, Y. Ma, L. Niu, Defective vs high-quality graphene for solid-contact ion-selective electrodes: effects of capacitance and hydrophobicity, *Electrochem. Commun.* 129 (2021), 107091.
- [40] M.K.A. El-Rahman, M.R. Rezk, A.M. Mahmoud, M.R. Elghobashy, Design of a stable solid-contact ion-selective electrode based on polyaniline nanoparticles as ion-to-electron transducer for application in process analytical technology as a real-time analyzer, *Sens. Actuators B* 208 (2015) 14–21.
- [41] B. Hambly, M. Guzinski, B. Pendley, E. Lindner, Evaluation, pitfalls and recommendations for the “water layer test” for solid contact ion-selective electrodes, *Electroanalysis* 32 (2020) 781–791.
- [42] T. Lindfors, J. Szucs, F. Sundfors, R.E. Gyurcsanyi, Polyaniline nanoparticle-based solid-contact silicone rubber ion-selective electrodes for ultratrace measurements, *Anal. Chem.* 82 (2010) 9425–9432.
- [43] A.E. Ibrahim, S.E. Deeb, E.M. Abdelhalim, A. Al-Harrasi, R.A. Sayed, Green stability indicating organic solvent-free HPLC determination of Remdesivir in substances and pharmaceutical dosage forms, *Separations* 8 (2021) 243.
- [44] B. Várnai, M. Malanga, T. Sohajda, S. Béni, Molecular interactions in remdesivir-cyclodextrin systems, *J. Pharm. Biomed. Anal.* 209 (2022), 114482.
- [45] K. Tohda, D. Drago, M. Shibata, Y. Umezawa, Studies on the matched potential method for determining the selectivity coefficients of ion-selective electrodes based on neutral ionophores: experimental and theoretical verification, *Anal. Sci.* 17 (2001) 733–743.
- [46] Y. Umezawa, K. Umezawa, H. Sato, Selectivity coefficients for ion-selective electrodes: recommended methods for reporting KA, Bpot values (Technical Report), *Pure Appl. Chem.* 67 (1995) 507–518.
- [47] S.M. Hamza, N.M. Rizk, H.A. Matter, A new ion selective electrode method for determination of oseltamivir phosphate (Tamiflu) and its pharmaceutical applications, *Arab. J. Chem.* 10 (2017) S236–S243.
- [48] M.N.d. Silva, Biowaiver monographs for immediate-release solid oral dosage forms: oseltamivir phosphate—a draft document, (2016).
- [49] S. Ide, S. Saito, T. Akazawa, T. Furuya, J. Masuda, M. Nagashima, Y. Asai, T. Ogawa, R. Yamamoto, H. Ishioka, Extracorporeal membrane oxygenation may decrease the plasma concentration of remdesivir in a patient with severe coronavirus disease 2019, *IDCases* 26 (2021) e01343.
- [50] X. Wang, L. Wang, C. Yao, G. Xie, S. Song, H. Li, Y. Qu, X. Tao, Novel formulations of the antiviral drug favipiravir: improving permeability and tabletability, *Cryst. Growth Des.* 21 (2021) 3807–3817.
- [51] E.-P. National Center for Biotechnology Information. “PubChem Compound Summary for CID 145996610, <https://pubchem.ncbi.nlm.nih.gov/compound/eidd-2801>. Accessed 4 March, 2023.
- [52] W.-J. Hu, L. Chang, Y. Yang, X. Wang, Y.-C. Xie, J.-S. Shen, B. Tan, J. Liu, Pharmacokinetics and tissue distribution of remdesivir and its metabolites nucleotide monophosphate, nucleotide triphosphate, and nucleoside in mice, *Acta Pharmacol. Sin.* 42 (2021) 1195–1200.